Journal of Systems Engineering and Electronics
Vol. 32, No. 5, October 2021, pp.1041 – 1052

A fault-tolerant control method for distributed flight control system facing wing damage

CUI Yuwei[1,2,*], LI Aijun[1], and MENG Xianfeng[2]

1. School of Automation, Northwestern Polytechnical University, Xi'an 710072, China;
2. Aviation Industry Corporation of China Xi'an Flight Automatic Control Research Institute, Xi'an 710065, China

Abstract: With the strong battlefield application environment of the next generation fighter, based on the design of distributed vehicle management system, a fault diagnosis and fault-tolerant control (FTC) method for wing surface damage is proposed in this paper. Aiming at three kinds of wing damage modes, this paper proposes a diagnosis method based on the fault decision tree and forms a fault decision tree for wing damage from the aspects of sample database construction, feature parameter extraction, and fault decision tree construction. Based on the fault diagnosis results, the longitudinal control law based on dynamic inverse and the lateral-directional robust control laws based on linear quadratic regulator (LQR) are proposed. From the simulation examples, the fault diagnosis algorithm based on the decision tree can complete the judgment of three wing surface damage modes within 2 ms, and the FTC law can make the fighter quickly return to a stable flight state after a short transient of 1 s, which achieves the fault-tolerant goal.

Keywords: flight control, fault diagnosis, distributed system, dynamic inverse, linear quadratic regulator (LQR).

DOI: 10.23919/JSEE.2021.000089

1. Introduction

In recent years, the development program for the next generation fighter aircraft has been rolled out. In April 2018, Europe's Airbus and France's Dassault jointly announced the future combat aviation system (FCAS), which consists of next-generation fighters, long-endurance UAVs, and swarm UAVs. Following the presentation of the next generation aircraft program at Farnborough Airshow in July 2018, in July 2020 the UK Air Force unveiled design concepts for the Tempest fighter and the lightweight affordable novel combat aircraft (LANCA) in support of a combination of manned and unmanned controls. The United States initiated the Loyalty Wingman Program, or MQ58A, which began joint operational technical verification with manned F-15X, F-35, and F-22 fighters. Russia has proposed a manned/unmanned hybrid fleet of fighters and in 2020 demonstrated a loyal wingman at thunderbolt high speed with no one to watch. Thus, the manned/unmanned combination has become a feature of future wars [1−3]. At the same time, the future war mode is changing to the joint operation mode in a multi-dimensional and complex environment. Manned fighter aircraft at the core of the fighter fleet must have enough survivability in a high-intensity battlefield environment [4,5]. Therefore, in addition to requiring the fighter to achieve extremely low detectability, higher requirements are also put forward for the flight control system, that is, sufficient fault tolerance is required, especially for possible critical wing surface damage.

Fortunately, key technologies are advancing [6−9]. Based on the network distributed system structure, the research on and application in the safety flight critical system are more and becoming more extensive [10−12]. It can realize that the whole task of the system is not affected after the failure of some control computers. Intelligent sensor technology has also been developed rapidly. After a redundancy sensor fails, information redundancy can be provided by redundancy information, and the sensor that fails can be compensated by signal reconstruction [13,14]. Electro-hydrostatic actuation technology with distributed hydraulics [15,16], or even high-power all-electric actuation technology, no longer requires the centralized supply of pressure for the steering gear through a unified hydraulic source, which provides possibility of fault tolerance after partial damage of aircraft wings and rudder surface. The development of these technologies provides good conditions for the flight control system to realize fault-tolerant control with wing damage.

Most importantly, in order to achieve better control characteristics of the aircraft after wing surface damage,

Manuscript received December 28, 2020.
*Corresponding author.
This work was supported by the Defense Industrial Technology Development Program (JCKY2016205C013).

ensure certain flight quality and the command role manned fighters play, and at least achieve safe return, it is necessary to solve the problem of fault detection and fault-tolerant control (FTC) of the aircraft wing surface damage in a strong battlefield environment. At present, the research about FTC after battle damage mainly focuses on the control methods, including model reference adaptive control and L1 adaptive applications [17−21], and the algorithm complexity is high. However, there is no consideration about the control architecture toward the fault-tolerant flight control system. Meanwhile, studies on fault detection after the wing surface damage are scarce.

This article is application-oriented from the perspective of system. It puts forward a flight control system scheme. The system structure distributed through the network, the intelligent sensor, the distributed computer network interconnection, and the servo control terminal form a whole system network connection which can adapt to the system fault in the computer's battle damage. From the view of fault detection, a fast identification method for wing surface damage is proposed, and a classification method based on decision tree is used to study various possible fault modes. An FTC law design for wing surface damage is presented, and the control compensation for wing surface damage is realized by longitudinal dynamic inverse control law structure and lateral-directional linear quadratic regulator (LQR) based robust control law structure. As a whole, the technical scheme for a new flight control system (FCS) is formed.

2. General description of the FCS

With the continuous deepening of the function integration of each aircraft subsystem, the flight control system has gradually developed into the vehicle management system, realizing the integration of several aircraft subsystems including the flight control system, the engine control system, the electromechanical control system, and other key flight safety systems.

Firstly, the network distributed system structure plays a key role in the functional integration of aircraft subsystems, as shown in Fig. 1. By connecting each control computer to the system network, the basis of information interaction of each subsystem can be achieved, and the functional integration of the complex large system can be realized. Firstly, the network distributed system structure plays a key role in the functional integration of each subsystem of the aircraft. The vehicle management system is mainly composed of three functional modules. Intelligent sensor module is composed of the plane of every smart sensor for each subsystem, including the angular velocity sensor and acceleration sensor for the flight control system, and the brake sensor and turning sensor required by the electromechanical system. The core computing module is composed of distributed core computers, which constitute the control core. In addition to completing routine information acquisition, control law solving, and control instruction output, it also completes the FTC function of the system. The servo drive module is composed of various controllable drive actuators, including elevator, aileron, and rudder driven by the flight control system, throttle lever and fuel saving valve driven by the engine control system, front wheel turning mechanism and brake mechanism driven by the mechanical and electrical system, etc.

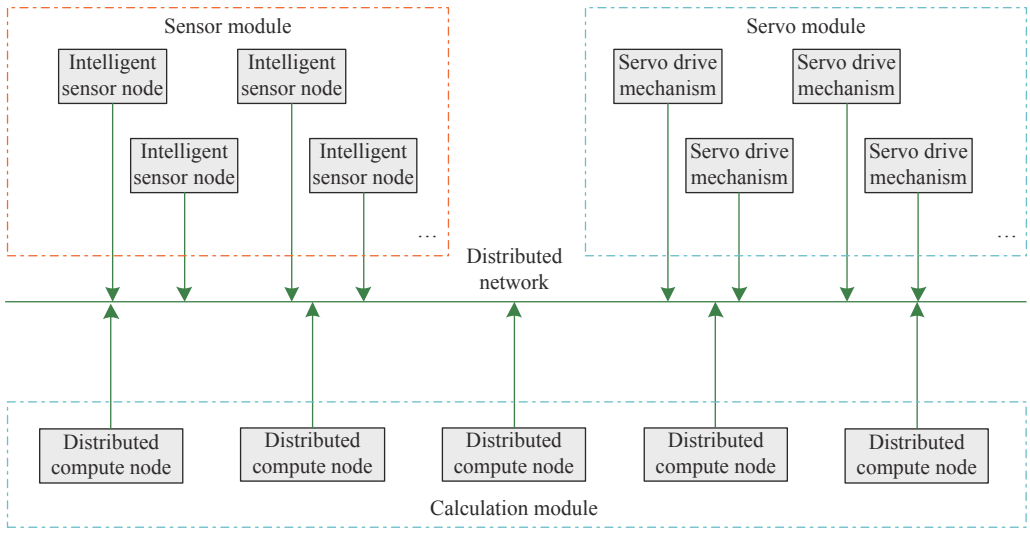

Fig. 1 Distributed system structure diagram

The biggest technical superiority of the network distributed system structure is that the computers are connected by the distributed network, thus, the aircraft subsystem functions are integrated, and the task scheduling

through the network can be done when a computer or a few computers malfunction, which ensure the orderly operation of the whole system. This provides a guarantee for the system mission operation after the occurrence of control computer damage or malfunction which may be caused by war damage.

Secondly, the servo drive mechanism involves miniaturization, high-power, intelligent, distributed hydraulic or electric actuator technology direction. In these devices, the servo drive mechanism not only contains the mechanical drive part, but also concentrates the hydraulic energy or the electrical energy components. For example, electrical hydrostatic actuator (EHA) and electromechanical actuator (EMA). The F-35 is the first fighter to use multi-electric technology, and it is an ingenious application of the "power-by-wire" technology, specifically, a high-power electrical system consisting of 270 V high voltage and a compact image-functional EHA, as shown in Fig. 2. It cancelled some complicated and heavy maintenance and delicate hydraulic mechanism. More importantly, with the concept of distributed energy, the servo actuator only needs to obtain the control instruction from the control computer, and energy is performed by their own structures. Thus, the system becomes more decoupled and more reliable, which reduces the impact as much as possible after damage of a servo actuator in the wing occurs.

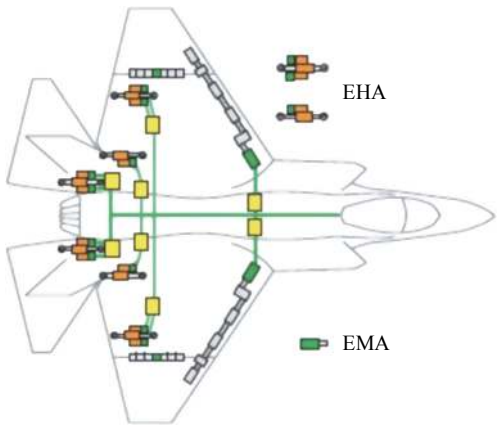

Fig. 2 F-35's EHA and EMA distribution diagram

In this paper, based on the above two conditions, the design of the flight control system adopts the network distributed system structure, so that the computing network of the system has the fault-tolerant ability in case of the damage of some computers. EHA or EMA is used to ensure isolation of servo actuators in the case of damage.

This paper considers the above aircraft configurations in Table 1 and discusses the problem of wing surface damage fault detection and FTC under multiple damage modes. The aircraft has several main control surfaces, including the inner elevator, the outer ailerons, and the rudder, as shown in Fig. 3. And the paper considers the most common patterns of wing damage: 50% right wing damage, 50% vertical tail damage, and 95% vertical tail damage, as shown in Table 2.

Table 1 Geometric parameters of the aircraft

Main parameter	Value
Length/mm	2 426
Wingspan/mm	2 000
Wing area/m^2	0.72
Weight/kg	21
Maximum thrust/kg	20

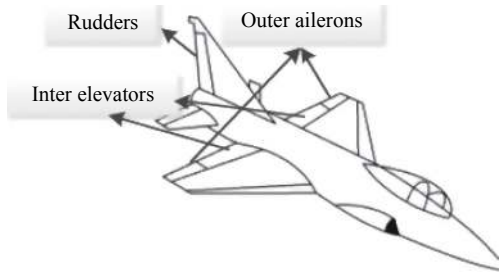

Fig. 3 Control surfaces of the aircraft discussed

Table 2 Configuration of wing damage

Configuration number	Detailed parameter
No.1	No damage
No.2	50% right wing damage
No.3	50% vertical tail damage
No.4	95% vertical tail damage

3. Fault diagnosis based on the decision tree

In the fault diagnosis problems of complex systems, diagnostic capacity mainly depends on the knowledge. However, because of the bottleneck of knowledge acquisition, the knowledge of diagnosis system is usually incomplete; therefore, a good diagnosis system should have certain learning ability and adaptive ability in the face of the new samples. Decision tree learning is a sample-based inductive learning method. It is one of the most important methods in machine learning and also the most common and effective method in the process of knowledge acquisition.

The fault diagnosis based on the decision tree can obtain the fault diagnosis knowledge rules by learning the fault sample set, solving the problem of knowledge acquisition bottleneck, and ensuring the further knowledge accumulation. At the same time, according to the exist-

ing knowledge rules in the knowledge base, the reasoning ability can be used to analyze the causes of faults during fault monitoring, so as to achieve fault diagnosis.

As a typical classification method, fault diagnosis based on the decision tree is powerful and easy to extract rules. An induction algorithm is used to generate the decision tree, in which each path represents a rule. The following steps are required for the fault diagnosis of wing surface damage by adopting the fault diagnosis based on the decision tree:

Step 1 Accumulate sample data of various damage configurations.

Step 2 The characteristic parameters of each damage configuration are mined from the sample data.

Step 3 The algorithm rules of the decision tree are summarized to form the decision tree of fault diagnosis.

3.1 Building the sample database

For the fault diagnosis of wing damage, the sample database is the dynamic change of aircraft input and output signals under various damage configurations.

In order to obtain more extensive sample data, this paper collects the sample database of the aircraft by injecting various damage configurations into the mathematical model of the aircraft described in Fig. 3 in Section 2.

In this paper, the flight envelope containing the following eight state points is considered, as shown in Table 3.

Table 3 Condition point considered in flight envelope

Condition point	Height/km	Velocity/km·h^{-1}
No.1	0.40	90.0
No.2	0.40	100.8
No.3	0.40	115.2
No.4	0.50	100.8
No.5	0.50	115.2
No.6	0.50	126.0
No.7	0.50	144.0
No.8	0.50	162.0

Assuming that the aircraft is in the state of altitude maintenance and roll attitude maintenance, a certain wing damage configuration occurs at a certain time. By observing and counting the response characteristics of the aircraft at the time of damage, it can be found that:

First, the damage configuration of the right wing will lead to lift loss and additional roll moment. Therefore, it has a great influence on the longitudinal and lateral-directional response, especially the longitudinal response.

Second, the damage configuration of vertical tail mainly affects lateral-directional characteristics, especially when vertical tail loses 95%, it will lead to drastic changes of lateral-directional characteristics.

Therefore, these three damage configurations all lead to drastic changes in aircraft response and diverging to an uncontrollable state in a very short time. When similar structural damage occurs to the aircraft, the damage configuration must be detected quickly and appropriate control laws must be adopted to keep the aircraft in a stable flight state.

Take the condition point No.1 as an example. When the wing damage occurs in 6 s, its response characteristics is shown in Fig. 4 below. V and H represent flight speed and altitude respectively; α and β represent angle of attack and sideslip angle respectively; p, q, and r represent the roll angle rate, the pitch angle rate, and the yaw angle rate respectively; θ and ϕ represent the pitch angle and the roll angle respectively; δ_a, δ_e, and δ_r, represent the amount of deflection of the outer aileron, the inner elevator, and the rudder respectively, and $\boldsymbol{\delta} = \left[\begin{array}{ccc} \delta_a & \delta_e & \delta_r \end{array} \right]^{\mathrm{T}}$.

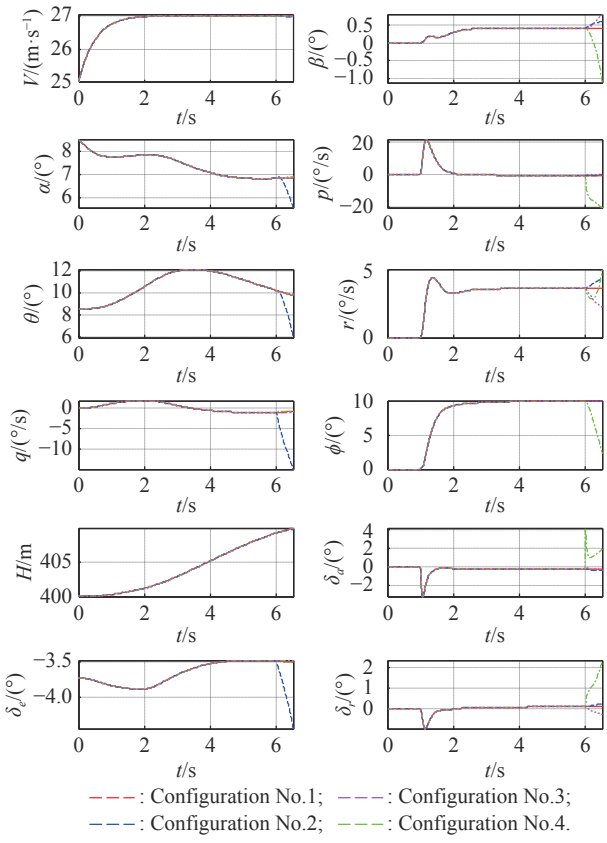

Fig. 4 Response graph of condition point No.1

3.2 Extracting the feature parameters

By processing each state signals and control surface deflection signals, an interesting phenomenon can be found. And it is also the key step of feature parameter extraction

in this paper. The acceleration values of these signals are extracted at the moment of damage. The acceleration values of the aircraft's various state signals and control surface deflection signals will change dramatically, and the signals affected by different damage configurations are not the same. For example, the unilateral wing damage has a severe impact on the change of the acceleration value of each longitudinal state signals and control surface deflection signals, resulting in pulse-type jump, while the vertical tail damage mainly causes the drastic change of each lateral-directional state signal and control surface deflection signal, which also results in pulse-type jump.

Take the condition point No.1 as an example. The acceleration values of changes in each state signals and control surface deflection signals are shown in Fig. 5.

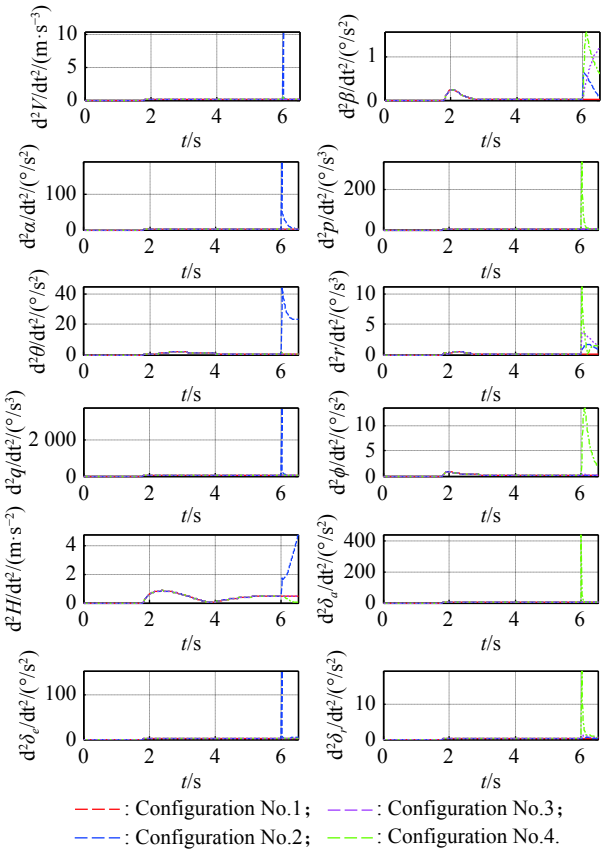

Fig. 5 Signal change acceleration values of condition point No. 1

According to a comprehensive simulation analysis, when the damage occurs, the acceleration values will change dramatically, and the values affected by different damage configurations are not the same. According to the eight condition points of the flight envelope, the acceleration values of each signal are collected in Fig. 6.

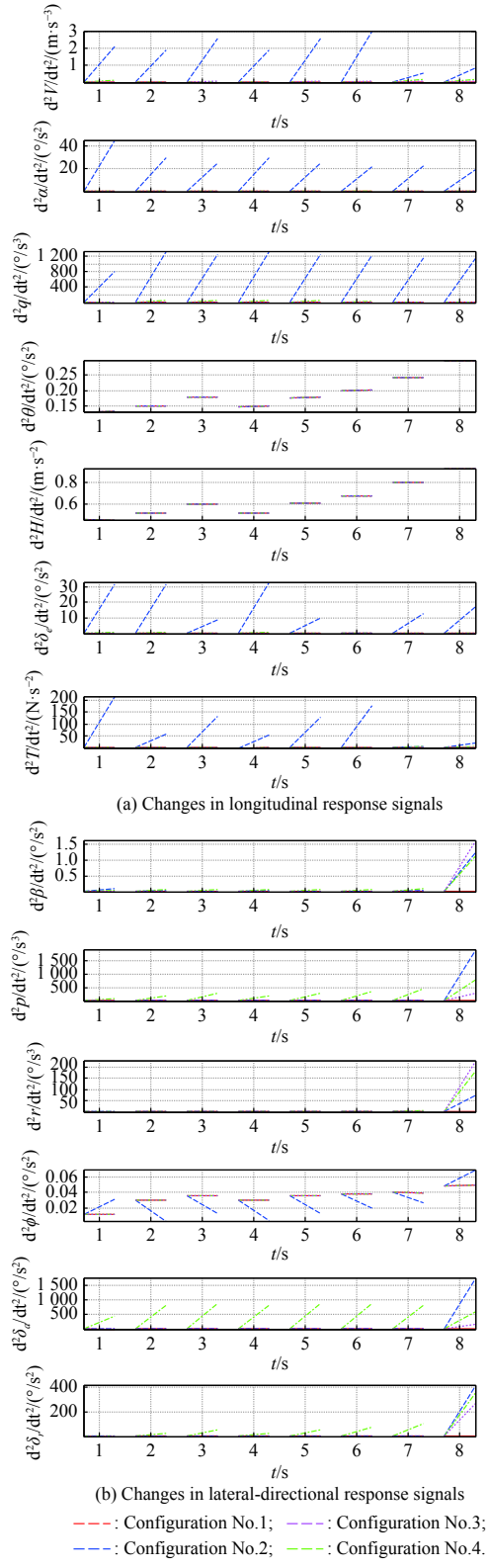

Fig. 6 Signal change acceleration values of eight condition points

In Fig. 6, the abscissa is the condition point number, and the line segment is the acceleration change value of each signal before and after the damage of the wing.

Among them, the left endpoint is the signal value before the damage, and the right endpoint is the signal value after the damage.

Based on the learning method of the decision tree, a large number of data samples are needed to run the data mining algorithm. Theoretically, the more data samples there are, the more accurately the characteristics of each class can be reflected, and the smaller the classification error will be. Therefore, according to all the sample data of the eight conditions points in the flight envelope, this paper selects two speed commands (no change in speed commands and 1 m/s change in speed commands), and generates 82 sample instances under each sample input condition for 12 sample input conditions as shown in Table 4. Therefore, a total of 768 sample instances are generated. In fact, the sample database is large enough and the more samples it contains, the more accurately it can reflect the characteristics of various damage configurations, and the smaller the error of fault diagnosis will be.

Table 4 Sample input conditions

Roll angle command/(°)	Height command/m		
	0	5	30
0	Sample 1	Sample 2	Sample 3
5	Sample 4	Sample 5	Sample 6
10	Sample 7	Sample 8	Sample 9
30	Sample 10	Sample 11	Sample 12

By the analysis according to Section 3.2 for the feature parameters, eight kinds of feature signals are extracted as the marks of fault feature modes and constitute the fault identification parameter sets, whcih are the angle of attack response, the pitching angle velocity response, the elevator response, the thrust response, the roll angle rate response, the yaw angular rate response, the aileron response, and the rudder response. The 768 samples not only include the fault data of normal configuration and damage configuration, but also cover the characteristics with different control command combinations.

3.3 Constructing the decision tree

Decision tree construction algorithms include ID3, C4.5, and classification and regression tree (CART). The ID3 algorithm is mainly used for the attribute selection problem, which is one of the most influential and the most typical algorithms. In each node of the tree, an attribute is found, and it is the best to classify the training set. ID3's defect is that it tends to have a large number of attribute values. In this paper, the attributes of the feature parameters under the three damage configurations of the aircraft in the decision tree are classified by two dichotomy methods (with only two values {0,1}), and the dichotomy characteristics can well avoid the defects of the ID3 gain measurement bias algorithm. The detail of the algorithm is described as follows:

Step 1 Create a root node for the decision tree toward the examples.

Step 2 If all examples are positive, return the single-node tree root, with label=label+1.

Step 3 If all examples are negative, return the single-node tree root, with label=label−1.

Step 4 If the number of predicting attributes is empty, then return the single node tree root, with label being the most common value of the target attribute in the examples.

Step 5 Otherwise, perform the following actions:

(i) Put the attribute that best classifies examples as A;

(ii) Assign A to the tree attribute for root;

(iii) For each possible value i of A, add a new tree branch below the root, corresponding to the test $A=i$;

(iv) Let example (i) be the subset of examples that have the value i for A;

(v) If example (i) is empty, then below this new branch add a leaf node with label being the most common target value in the examples; else, below this new branch add the subtree.

Therefore, according to the response characteristics of various features, a fault decision tree can be combined to perform fault diagnosis of wing damage. The result of the decision tree is shown in Fig. 7. The acceleration signal of the attack angle is the root of the decision tree, and then the child nodes and the final leaf nodes are constructed recursively with the same attribute selection algorithm on the basis of the two branches. In Fig. 7, δ_T represents the engine thrust.

In the process of decision tree construction, the decision attributes with high importance are located near the root node of the decision tree, and the values of these attributes have the greatest impact on the decision. Therefore, according to the generated decision tree knowledge base to assist fault diagnosis decision making, the quick decision tree structure is mainly used to analyze the process downwardly from more important attributes.

The structure of the decision tree results shows that traversing the entire decision tree down from the root, we are able to get classification rules. These rules reflect the features of fault, which can be used for fault diagnosis. Meanwhile, the decision tree can also be trained by rules applied to other expert system to provide the decision basis.

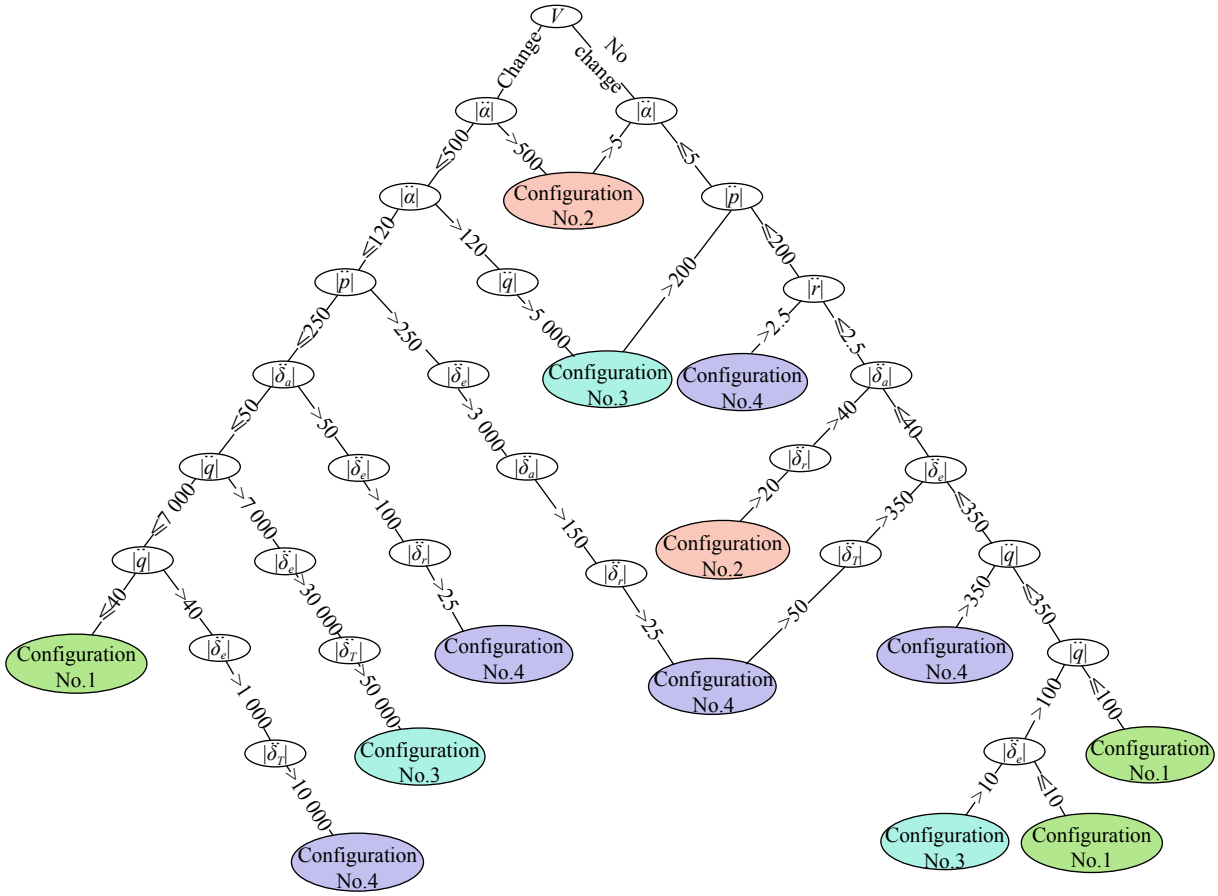

Fig. 7 Fault diagnosis decision tree

4. FTC law for wing damage

The biggest difference between the conventional control law and the FTC law is that the design should consider not only the state of all points within a certain flight envelope, but also the control law for a variety of damage configuration. Each kind of configurations of the aircraft should be able to reach a certain flight quality. That is, it needs to have strong robustness. In other words, the structure and parameters of the control law used in this paper need to adapt to the control requirements of multiple state points in normal configurations and multiple fault configurations.

Through the preliminary analysis of the damaged configuration, it can be found that:

(i) Under the normal condition where the aircraft is without damage, the longitudinal and lateral-direction are stable, and damping and frequency are within a normal range.

(ii) When the vertical tail damage is 50%, the dutch roll mode frequency is reduced by about 60%, and the aircraft is in a controllable state.

(iii) When the vertical tail damage is 95%, the aircraft is unstable lateral-directionally, with longitudinal and lateral-directional coupling, and the aircraft is uncontrollable.

(iv) When the right wing is damaged by 50%, the aircraft is unstable longitudinally and lateral-directionally, and the aircraft cannot be controlled.

It can be seen that when the wing of the aircraft is damaged, the longitudinal and lateral-directional stability is greatly reduced. Therefore, the control laws are needed to realize a normal flight of the aircraft. Through a large number of control law structures and parameter adjustments, this paper proposes a technical scheme of adopting a nonlinear control law structure based on dynamic inverse longitudinally and a robust control law structure based on LQR for lateral-directional acquisition.

4.1 Longitudinal control law based on dynamic inverse

The nonlinear dynamic inverse method has been relatively mature in theory. For aircraft objects, the input number of the system is generally smaller than the number of state variables of the system. Therefore, all state variables cannot be taken as outputs, and the solution is hier-

archical control.

(i) Fast variable loop design

Aircraft movement mainly depends on the deflection of the control surfaces, which produces torque and a small force. The torque can make the roll angular rate, the pitch angular rate, and the yaw angular rate change rapidly. Therefore, the fast variable loop composed of p, q, and r and can realize its accurate inverse with the angular acceleration generated by the control surface deflections. p, q, and r are the actual angular velocity feedbacks, which are measured by the aircraft sensor in real time. The equation of state is shown below.

$$\begin{bmatrix} p \\ q \\ r \end{bmatrix} = \begin{bmatrix} f_p(x_1) \\ f_q(x_1) \\ f_r(x_1) \end{bmatrix} + \boldsymbol{g}_1(x_1)\boldsymbol{\delta} \tag{1}$$

where $f(\cdot)$ and $g(\cdot)$ are the functions of the state vector.

For the aircraft model considered in this paper, the moment is mainly realized through the inner elevator, the outer aileron, and the rudder. Therefore, the solution of the inner loop can be obtained as follows:

$$\begin{bmatrix} \delta_e \\ \delta_a \\ \delta_r \end{bmatrix} = \boldsymbol{g}_1^{-1}(x_1)\left(\begin{bmatrix} p_d \\ q_d \\ r_d \end{bmatrix} - \begin{bmatrix} f_p(x_1) \\ f_q(x_1) \\ f_r(x_1) \end{bmatrix}\right), \tag{2}$$

$$\begin{cases} p_d = \omega_p(p_c - p) \\ q_d = \omega_q(q_c - q) \\ r_d = \omega_r(r_c - r) \end{cases}, \tag{3}$$

where p_c, q_c, and r_c are the input control instruction of the loop, ω_p, ω_q, and ω_r are the expected bandwidth values. The fast variable loop control law structure obtained thus is shown in Fig. 8.

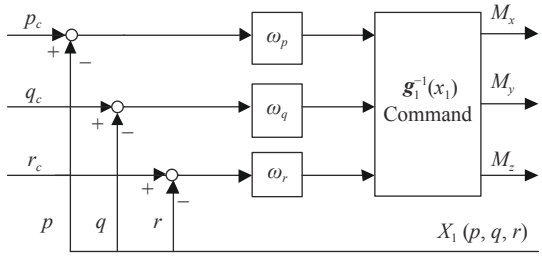

Fig. 8 Fast variable loop control structure

(ii) Sub-fast variable loop design

The aerodynamic force has little influence on α, β, and ϕ, but angular rates have significant influence on them. That is to say, angular acceleration generated by the deflection of the control surface mainly has effect on $\mathrm{d}\alpha/\mathrm{d}t$, $\mathrm{d}\beta/\mathrm{d}t$, and $\mathrm{d}\phi/\mathrm{d}t$. Therefore, we ignore the force generated by the aerodynamic force, and the results generated by fast variable p, q, and r are approximate inverses.

The equation of the state can be rewritten as follows:

$$\begin{bmatrix} \alpha \\ \beta \\ \phi \end{bmatrix} = \begin{bmatrix} f_\alpha(x_2) \\ f_\beta(x_2) \\ f_\phi(x_2) \end{bmatrix} + \boldsymbol{g}_2(x_2)\begin{bmatrix} p \\ q \\ r \end{bmatrix}. \tag{4}$$

By inverting the above formula, three command angular accelerations can be obtained as follows:

$$\begin{bmatrix} p_d \\ q_d \\ r_d \end{bmatrix} = \boldsymbol{g}_2^{-1}(x_2)\left(\begin{bmatrix} \alpha_d \\ \beta_d \\ \phi_d \end{bmatrix} - \begin{bmatrix} f_\alpha(x_2) \\ f_\beta(x_2) \\ f_\phi(x_2) \end{bmatrix}\right), \tag{5}$$

$$\begin{bmatrix} \alpha_d \\ \beta_d \\ \phi_d \end{bmatrix} = \begin{bmatrix} \omega_\alpha(\alpha_c - \alpha) \\ \omega_\beta(\beta_c - \beta) \\ \omega_\phi(\phi_c - \phi) \end{bmatrix}, \tag{6}$$

where α_c, β_c, and ϕ_c are the input control command of the loop that describes the attitude angle that the aircraft needs to maintain in order to track a predetermined flight path. α and β are the actual flow angle feedback. ϕ is the actual roll angle feedback which is measured by real-time sensors. The structure of the sub-fast variable loop control law is shown in Fig. 9.

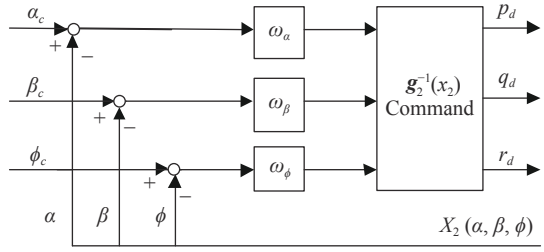

Fig. 9 Sub-fast variable loop control structure

(iii) Slower variable loop design

Further inward, the bandwidth of flight speed V, flight azimuth angle γ, and the flight track roll angle χ is 0.2−0.5 rad/s, which are usually used as a slower variable loop. The throttle command generates thrust to control the speed, while ignoring the force generated by the control surface.

Construct the desired derivative value from the input command and the actual flight data feedback:

$$\begin{bmatrix} V_d \\ \gamma_d \\ \chi_d \end{bmatrix} = \begin{bmatrix} \omega_v(V_{dc} - V_d) \\ \omega_\gamma(\gamma_{dc} - \gamma_d) \\ \omega_\chi(\chi_{dc} - \chi_d) \end{bmatrix}, \tag{7}$$

$$\begin{bmatrix} V_d \\ \gamma_d \\ \chi_d \end{bmatrix} = \begin{bmatrix} f_V(x_3) \\ f_\gamma(x_3) \\ f_\chi(x_3) \end{bmatrix} + \boldsymbol{g}_3(x_3)\begin{bmatrix} \alpha \\ \beta \\ \varphi \end{bmatrix}. \tag{8}$$

The desired angular acceleration can then be calculated to provide the torque value of the control surface:

$$\begin{bmatrix} \alpha_d \\ \beta_d \\ \varphi_d \end{bmatrix} = \begin{bmatrix} \alpha \\ \beta \\ \varphi \end{bmatrix} = \boldsymbol{g}_3^{-1}(x_3)\left(\begin{bmatrix} V_d \\ \gamma_d \\ \chi_d \end{bmatrix} - \begin{bmatrix} f_V(x_3) \\ f_\gamma(x_3) \\ f_\chi(x_3) \end{bmatrix}\right). \tag{9}$$

The structure of the slower variable loop is shown in Fig. 10.

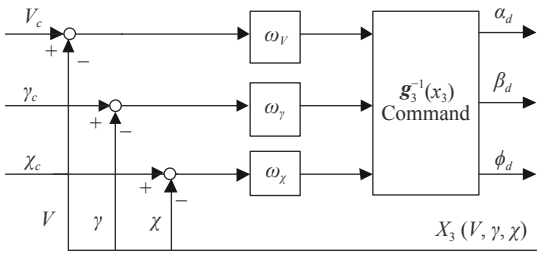

Fig. 10 Slower variable loop control structure

(iv) Slow variable loop design

Finally, the displacement variable of the aircraft x, y, and z is the slow variable loop.

The expected derivative value is constructed from the input command and the actual flight data feedback:

$$\begin{bmatrix} x_d \\ y_d \\ z_d \end{bmatrix} = \begin{bmatrix} \omega_x(x_{dc}-x_d) \\ \omega_y(y_{dc}-y_d) \\ \omega_z(z_{dc}-z_d) \end{bmatrix}, \tag{10}$$

$$\begin{bmatrix} x \\ y \\ z \end{bmatrix} = \begin{bmatrix} f_x(x_4) \\ f_y(x_4) \\ f_z(x_4) \end{bmatrix} + \boldsymbol{g}_4(x_4) \begin{bmatrix} V \\ \gamma \\ \chi \end{bmatrix}. \tag{11}$$

Solve (11) to obtain the output instruction of the loop:

$$\begin{bmatrix} V_d \\ \gamma_d \\ \chi_d \end{bmatrix} = \begin{bmatrix} V \\ \gamma \\ \chi \end{bmatrix} = \boldsymbol{g}_4^{-1}(x_4) \left(\begin{bmatrix} x_d \\ y_d \\ z_d \end{bmatrix} - \begin{bmatrix} f_x(x_4) \\ f_y(x_4) \\ f_z(x_4) \end{bmatrix} \right). \tag{12}$$

The structure of the slow variable loop is shown in Fig. 11.

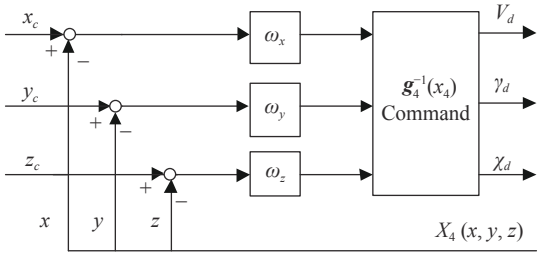

Fig. 11 Slow variable loop control structure

In this way, the dynamic characteristics of aircraft are divided into four subsystems, and the flight control law structure also forms a four-layer feedback structure. Based on this, the longitudinal control law completes the design of control functions such as height maintenance and pitch attitude maintenance. To be specific, the control law block diagram is shown in Fig. 12. H_c and V_c are the reference height and reference speed respectively. θ and α_0 are the angle of pitch and the trim angle of attack respectively. Then, the output δ_e of the control module is the deflection angle of elevator.

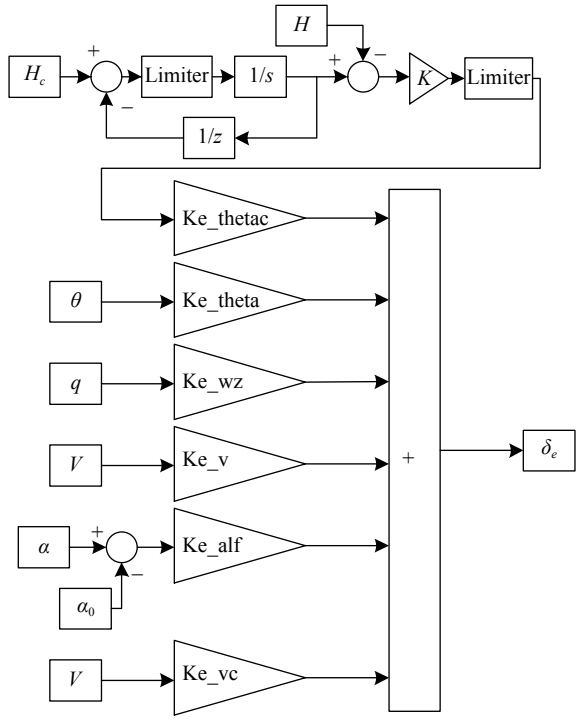

Fig. 12 Longitudinal control law block

4.2 Lateral-directional robust control law based on LQR

Define linear time-invariant systems that can be controlled and observed:

$$\begin{cases} \boldsymbol{x}(t) = \boldsymbol{A}\boldsymbol{x}(t) + \boldsymbol{B}\boldsymbol{u}(t), \boldsymbol{x}(t_0) = \boldsymbol{x}_0 \\ \boldsymbol{y}(t) = \boldsymbol{C}\boldsymbol{x}(t) + \boldsymbol{D}\boldsymbol{u}(t) \end{cases}. \tag{13}$$

where, $\boldsymbol{A}$, $\boldsymbol{B}$, $\boldsymbol{C}$, and $\boldsymbol{D}$ are the state coefficient matrix, the control coefficient matrix, the output state coefficient matrix, and the output control coefficient matrix, respectively. Take the expected time-domain performance index of the aircraft as the target, and define the state regulation performance index J in the quadratic form:

$$J = \frac{1}{2}\int_0^\infty \left[\boldsymbol{x}^{\mathrm{T}}(t)\boldsymbol{Q}\boldsymbol{x}(t) + \boldsymbol{u}^{\mathrm{T}}(t)\boldsymbol{R}\boldsymbol{u}(t) \right] \mathrm{d}t \tag{14}$$

where $\boldsymbol{Q}$ is semidefinite symmetric constant matrix, and $\boldsymbol{R}$ is the positive definite real symmetric constant matrix, which are weighted matrices selected by demand.

Then the optimal control exists and is uniquely determined by the following formula:

$$\boldsymbol{u}(t) = -\boldsymbol{R}^{-1}\boldsymbol{B}^{\mathrm{T}}\boldsymbol{P}\boldsymbol{x}(t). \tag{15}$$

Thus, the state feedback gain $\boldsymbol{K}$ can be obtained, and $\boldsymbol{P}$ is the constant positive definite matrix satisfying the Riccati equation:

$$\boldsymbol{K} = -\boldsymbol{R}^{-1}\boldsymbol{B}^{\mathrm{T}}\boldsymbol{P} \tag{16}$$

Design the feedback gain $\boldsymbol{K}$ to minimize the performance index and to ensure that the control energy used and the state of the aircraft oscillations are minimal. And, the most important thing is that the control law based on the LQR method guarantees the stability under certain conditions. Thus, its robust stability performance is also very attractive, and it is more crucial for FTC.

Based on this, the lateral-directional control law has completed the functional design of flight track angle holding and sideslip angle control. Specifically, the control law block diagram is shown in Fig. 13.

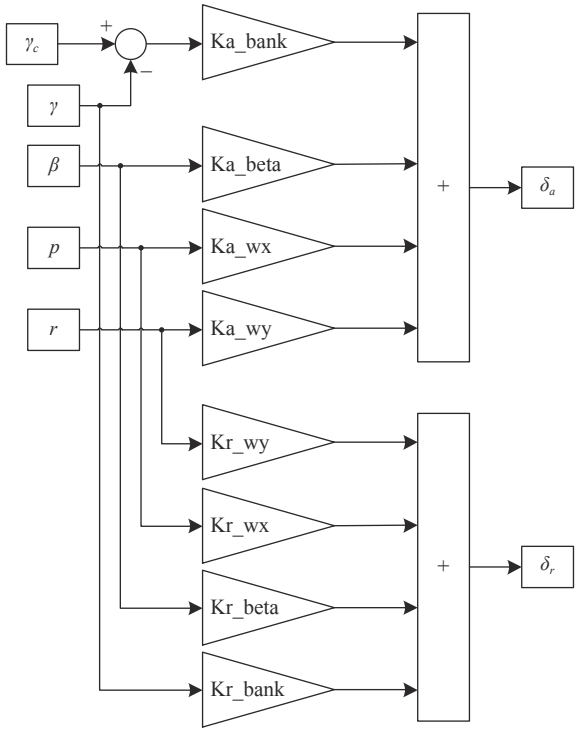

Fig. 13 Lateral-directional control law block

5. Simulation example

The aircraft described in Section 2 is taken as the simulation object, and the three fault modes of the right wing damage (50%), the vertical tail damage (50%), and the vertical tail damage (95%) are targeted. The fault diagnosis design based on the decision tree is used to carry out the simulation verification of wing damage. Based on the fault diagnosis results, the longitudinal control laws based on dynamic inverse and lateral-directional robust control law based on LQR are designed to carry out the simulation verification of FTC for wing damage.

Firstly, based on the description in Section 4, the control law parameters in the control law structure are given in Table 5 for the longitudinal ones, and in Table 6 for the lateral-directional ones, taking condition point No.1 as an example.

Table 5 Longitudinal control law parameter

Control law parameter	Parameter value
Ke_theta	0.0130
Ke_thetac	−0.0868
Ke_wz	0.0347
Ke_v	0.0120
Ke_alf	−4.2259
Ke_vc	3.3852

Table 6 Lateral-directional control law parameter

Control law parameter	Parameter value
Ka_beta	0.5111
Ka_wx	−0.2587
Ka_wy	−0.0791
Ka_bank	−0.3208
Kr_beta	0.0390
Kr_wx	0.0654
Kr_wy	−0.2319
Kr_bank	0.0764

The simulation scenario is described as follows: set the control command as $\Delta H_{\mathrm{cmd}} = 5\ \mathrm{m}, V_{\mathrm{cmd}} = V_0, \phi_{\mathrm{cmd}} = 5^\circ$, and the time of the wing damage (three configurations) is 6 s. The damage diagnosis time, the damage diagnosis results, and the response transient state of the aircraft within 1 s after the occurrence of the damage are recorded.

The following results are obtained:

(i) After the occurrence of the three kinds of damage of the aircraft, the time of fault diagnosis is 2 ms, that is, the diagnosis can be completed in the same cycle after the occurrence of damage.

(ii) The maximum transient states of the aircraft within 1 s after the damage of the three kinds of aircraft are very small. The transient change of the pitch angle rate is no more than 0.5 °/s, the transient change of the yaw angle rate is no more than 1.1 °/s, and the transient change of the roll angle rate is no more than 6 °/s.

(iii) After the damage occurs, the aircraft quickly recoveres a steady flight state after a short transient state, and the error between the control commands and responses is very small.

Take the condition point No.1 as an example, its response characteristics are shown in Fig. 14.

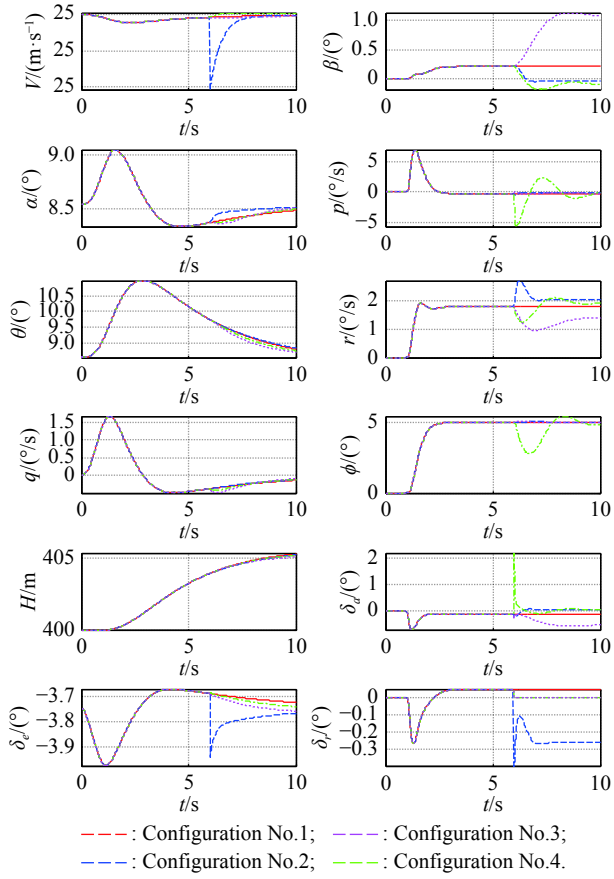

Fig. 14 FTC response graph of condition point No.1 after damage

6. Conclusions

The next generation aircraft is facing an intense battlefield environment. This paper proposes a technical scheme of distributed vehicle management system, from the perspective of the distributed computer, smart sensors, and EHA or EMA, and expounds the fault-tolerant ability of distributed control system, providing a good condition for FTC about the wing damage. This paper focuses on three wing damage modes, and develops fault diagnosis based on the decision tree learning. From the simulation example, we can see that the algorithm can complete online diagnosis within 2 ms with strong practicability. Based on the fault diagnosis results, this paper proposes the longitudinal flight control mechanism based on dynamic inverse and the lateral-directional robust flight control law based on LQR. The simulation example shows that it can quickly realize the aircraft stability control within 1 s after the wing damage, and has a small response transient.

References

[1] WANG X Y, CAO Y F, SUN H J, et al. Modeling for cooperative combat system architecture of manned/unmanned aerial vehicle based on DoDAF. Systems Engineering and Electronics, 2020, 43(10): 2265–2274. (in Chinese)

[2] LI L. Development analysis of typical manned/unmanned aerial vehicle collaborative operations projects abroad. Unmanned Systems Technology, 2020, 3(4): 83–90. (in Chinese)

[3] FAN J R, LI D G. Overview of MAV/UAV collaborative combat and its key technologies. Unmanned Systems Technology, 2019, 3(1): 39–47. (in Chinese)

[4] KIM K, KIM S, SUK J, et al. Flight test of flying-wing type unmanned aerial vehicle with partial wing-loss. Journal of Aerospace Engineering, 2019, 233(5): 1611–1628.

[5] KIM K, AHN J, KIM S, et al. Analysis of partial wing damage on flying-wing unmanned air vehicl. Journal of Aerospace Engineering, 2014, 228(3): 355–374.

[6] CHEN Z J, ZHANG R L, ZHANG P. Flight control: challenges and opportunities. Acta Automatica Sinica, 2013, 39(6): 703–710. (in Chinese)

[7] FAN Y M. Autonomous and intelligent control of the unmanned aerial vehicle. Science China−Technological Sciences, 2017, 47(3): 221–229.

[8] FAN Y M. The flight control technology and development. Aircraft Design, 2012, 32(4): 33–37. (in Chinese)

[9] WANG X Y, FANF H, DOU L H, et al. Integrated distributed formation flight control with aerodynamic constraints on attitude and control surfaces. Nonlinear Dynamics, 2018, 91: 2331–2345.

[10] XU Y L, CUI Y W, LUO C. Research advancement for the new generation of distributed vehicle management system. Proc. of the 37th Chinese Control Conference, 2018: 10088–10092.

[11] CUI Y W, ZHAN Z Y, LU Z R, et al. A task scheduling method for network distributed flight control system. Proc. of the Chinese Automation Congress, 2019: 480–483.

[12] CUI Y W, LI A J. Research on the key technologies of network distributed flight control system. Proc. of the Chinese Automation Congress, 2020: 6928–6931.

[13] PRABHU S, ANITHA G. An innovative analytic redundancy approach to air data sensor fault detection. The Aeronautical Journal, 2019, 124(1273): 346–367.

[14] VAN EYKEREN L, CHU Q P. Sensor fault detection and isolation for aircraft control systems by kinematic relations. Control Engineering Practice, 2014, 31: 200–210.

[15] LI Y, JIAO Z X, WANG Z M. Design, analysis, and verification of an electro-hydrostatic actuator for distributed actuation system. Sensors, 2020, 20(3): 634.

[16] WANG Z M, JIAO Z X, LI X L. Design and testing of a linear-driven electro-hydrostatic actuator. Journal of Dynamic Systems, Measurement, and Control, 2019, 141(12): 121009.

[17] YANG J, NA J, GAO G B. Robust model reference adaptive control for transient performance enhancement. International Journal of Robust and Nonlinear Control, 2020, 30(15): 6207–6228.

[18] ANDERSON R B, MARSHALL J A, L'AFFLITTO A, et al. Model reference adaptive control of switched dynamical systems with applications to aerial robotics. Journal of Intelligent & Robotic Systems, 2020, 100(4): 1–17.

[19] MA T. Extended filtering high-gain output feedback controller for a class of uncertain nonlinear systems subject to external disturbances. International Journal of Robust and Nonlinear Control, 2020, 30(11): 4397–4417.

[20] KOTARU P, EDMONSON R, SREENATH K. Geometric L_1 adaptive attitude control for a quadrotor unmanned aerial vehicle. Journal of Dynamic Systems, Measurement, and Control, 2020, 142(3): 031003.

[21] LIU Y Q, CHE J C, CAO C Y. Advanced autonomous underwater vehicles attitude control with L_1 backstepping adaptive control strategy. Sensors, 2019, 19(22): 4848.

Biographies

CUI Yuwei was born in 1986. He received his B.S. and M.S. degrees in control theory and control engineering from Northwestern Polytechnical University in 2009 and 2012, respectively. He is currently pursuing his Ph.D. degree at Northwestern Polytechnical University. His research interests include aircraft flight control system, fault diagnosis, and fault-tolerant control.

E-mail: cuiyuwei0505@mail.nwpu.edu.cn

LI Aijun was born in 1973. He received his B.S., M.S., and Ph.D. degrees in aircraft design from Northwestern Polytechnical University in 1995, 2000, and 2005, respectively. Currently he is a professor and doctoral supervisor at Northwestern Polytechnical University. His research interests include aircraft flight control and intelligent control.

E-mail: liaijun@nwpu.edu.cn

MENG Xianfeng was born in 1990. He received his B.S. and M.S. degrees in guidance, navigation, and control from Nanjing University of Aeronautics and Astronautics in 2012 and 2016, respectively. He is currently with Xi'an Flight Automatic Control Research Institute, Aviation Industry Corporation of China. His research interests include modeling of control systems and fault diagnosis.

E-mail: xfmeng@facri.com